33rd Annual International Conference of the IEEE EMBS
Boston, Massachusetts USA, August 30 - September 3, 2011

Automatic 3D graph cuts for brain cortex segmentation in patients with focal cortical dysplasia

Ivana Despotović, Ief Segers, Ljiljana Platiša, Ewout Vansteenkiste, Aleksandra Pižurica,
Karel Deblaere and Wilfried Philips

Abstract— **In patients with intractable epilepsy, focal cortical dysplasia (FCD) is the most frequent malformation of cortical development. Identification of subtle FCD lesions using brain MRI scans is very often based on the cortical thickness measurement, where brain cortex segmentation is required as a preprocessing step. However, the accuracy of the selected segmentation method can highly affect the final FCD lesion detection. In this work, we propose an improved graph cuts algorithm integrating Markov random field-based energy function for more accurate brain cortex MRI segmentation. Our method uses three-label graph cuts and preforms automatic 3D MRI brain cortex segmentation integrating intensity and boundary information. The performance of the method is tested on both simulated MR brain images with different noise levels and real patients with FCD lesions. Experimental quantitative segmentation results showed that the proposed method is effective, robust to noise and achieves higher accuracy than other popular brain MRI segmentation methods. The qualitative validation, visually verified by a medical expert, showed that the FCD lesions were segmented well as a part of the cortex, indicating increased thickness and cortical deformation. The proposed technique can be successfully used in this, as well as in many other clinical applications.**

I. Introduction

The latest studies indicate that one out of two hundred adults suffer from recurrent epilepsy [1]. About 30% of them are due to focal cortical dysplasia (FCD), which is a malformation of the cortical development in the brain. In clinical treatments, the FCD lesions often have to be removed by surgery and before this can be done, it is necessary to detect and delineate the lesions. However, FCD detection is a very challenging task and standard radiological MRI evaluation of the lesions still fails in many cases, because of the complexity of the cortex and subtle behavior of the lesions. Therefore, developing an automatic algorithm for FCD detection would be a very useful tool for clinical diagnoses and surgical planning.

On MRI scans, FCD lesions are typically characterized with the increased cortical thickness, blurring of the gray-white matter interface and hyperintensity signal in the lesion area. Examples of T1-weighted (T1-W) MR images with FCD lesions are shown in Fig. 1.

To date, several methods have been reported for detection and visual improvement of FCD lesions [2]–[5]. Very often,

I. Despotovic, Ief Segers, Ljiljana Platiša, E. Vansteenkiste, Aleksandra Pižurica, W. Philips are with Faculty of Electrical Engineering, Ghent University, TELIN-IPI-IBBT, Sint-Pietersnieuwstraat 41, 9000 Ghent, Belgium
K. Deblaere is with Ghent University Hospital, Department of Radiology, Ghent, Belgium
e-mail: ivana.despotovic@telin.ugent.be

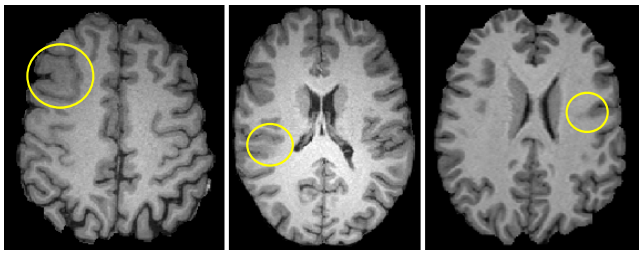

Fig. 1. Three examples of T1-weighted MRI with FCD lesions. The lesions are indicated with a circle. They are characterized by increased cortical thickness and blurring between gray matter and white matter.

the MRI scans are first preprocessed by removing skull, lipid layers and intensity inhomogeneity. Then, the maps of the three main FCD features are calculated: cortical thickness map, gradient map and relative intensity map. Cortical thickness measurement requires MRI to be segmented into: gray matter (GM, cortex), white matter (WM) and cerebrospinal fluid (CSF). Importantly, the final FCD detection results highly depend on the accuracy of the brain cortex segmentation, which is the focus of our work.

In general, accurate MRI brain cortex segmentation is a difficult task, not only because of the complicated structure of the brain and the anatomical variability between subjects, but also because of the presence of noise and low contrast between brain tissues in MRI. Since manual segmentation is time-consuming, prone to errors and subjective, automated and accurate tissue segmentation is needed.

Currently, the most popular methods used for brain cortex segmentation are the histogram-based method with automated threshold (HBM) [3], FMRIB's Automated Segmentation Tool (FAST-FSL) [6], Statistical Parametric Mapping (SPM) [7], Fuzzy C-Means (FCM) [8] and graph cuts [9], [10]. While most of these methods are suitable for general brain tissue segmentation, HBM is used in the vast majority of FCD detection techniques. The main disadvantage of the HBM method (as well as of the standard FCM method) is high sensitivity to noise and other imaging artifacts. In contrast, the FSL, SPM and graph cuts methods are less sensitive to noise because they include the spatial information of the neighboring pixels in the image segmentation. However, most of the segmentation techniques reach only local optimum in their stated energy function, while the graph cuts method is able to locate global minima for two-label energy functions and strong approximation to global minima for multi-label energy function [9], [11]. In this work,

978-1-4244-4122-8/11/$26.00 ©2011 IEEE

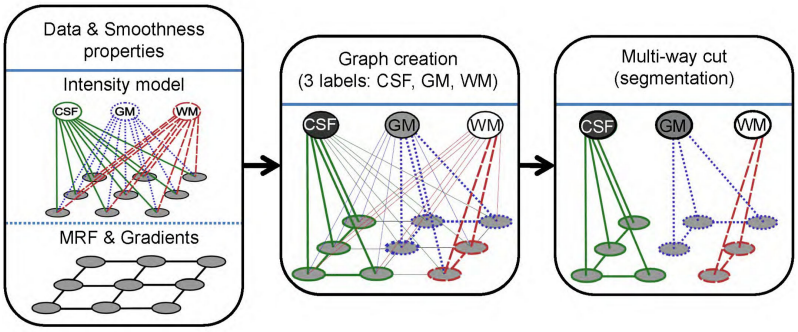

Fig. 2. Overview of the graph cuts segmentation for a 2D image with 3x3 pixels. In the first step, the two different types of edges of the graph are presented. The second step shows the complete graph. The edges between voxel nodes are initialized with weights that are calculated based on the smoothness properties (MRF and gradients). The weights for the edges between voxel nodes and labels are based on the data properties (intensity model). This is followed in the third module by the computation of an approximate multi-way cut, which results in a near global optimal segmentation.

we propose an improved graph cuts algorithm minimizing Markov random field-based (MRF-based) energy function for automatic brain cortex segmentation. Compared with previously proposed methods [10], [12], we do not use brain atlases for tissue segmentation (because we do not segment detailed brain structures) and our method is based on a three-label (WM, GM and CSF) brain segmentation using T1-W MRI scans, implemented in 3D (3DGC).

The paper is organized as follows: In Section II the proposed MRI segmentation algorithm is explained. Results are given in Section III and Section IV concludes this paper.

II. Method

Our technique is based on the graph cuts method proposed by Boykov and Jolly [9], [11]. They formulate segmentation as a problem of energy minimization, which can be solved by calculating the minimum cost cut in a graph, equal to the total energy of the corresponding segmentation.

Segmenting an image I into homogeneous regions of interest can be described as assigning a label $l_p \in L$ to each voxel $p \in I$. A graph cuts MRF-based energy function *E(l)* is formulated as:

$$E(l) = \lambda \sum_{p \in I} D_p(l_p) + \sum_{p,q \in N} V_{p,q}(l_p, l_q), \qquad (1)$$

where $D_p(l_p)$ is the data penalty function and measures how well the label l_p can be assigned to the voxel p based on observed data intensities and a chosen probabilistic model. The smoothness term $V_{p,q}(l_p, l_q)$ (interaction potentials) measures the neighborhood interaction by penalizing discontinuities between neighboring voxels pairs in a specified neighborhood system N. Parameter λ controls the relative importance of the data term with respect to the smoothness term. To optimize Eq. 1, a graph $G = \langle V, E \rangle$ consisting of set of nodes $v \in V$ and set of direct edges $e \in E$ is defined on image I. The nodes consist of image voxels and spacial terminal nodes (labels) L_i. There are two types of edges E defined on graph G: edges between each voxel node and terminal nodes and edges between neighboring voxels.

Here, we used an extended three-label graph cuts method where three terminal nodes $L_i \in \{L_{CSF}, L_{GM}, L_{WM}\}$ refer to the three brain tissue types: CSF, GM and WM. The flow of the corresponding graph construction is illustrated in Fig. 2. For simplicity, an example is given for a 2D image with 3×3 pixels. The first step involves the creation of the graph with two different set of edges. The first type of edges connect each voxel node v with each terminal node L_i and the second type of edges are those between two neighboring voxels in the defined neighbourhood system. This information corresponds to penalizations (costs or weights) on the edges and is computed based on an intensity model for the data term and additional gradient image for the smoothness term. The created graph is a three-terminal graph, shown in the second step. An optimal balance will be achieved by minimizing the energy function for all possible segmentations. The third step presents this minimization, that consists of the computation of an approximate multi-way cut.

The data properties are integrated by assuming a Gaussian mixture model (GMM) as intensity model. A GMM is fitted to the voxels intensity using the expectation-maximization (EM) algorithm [13]. In this way, the partial volume effects, that occur at the boundaries between tissues, are also taken into account. After the Gaussians are calculated, we have for each intensity value the probabilities of belonging to the three tissues $P_I(I_p|L_i)$. The data term $D_p(L_i)$ for a given label L_i is defined as the negative log-likelihood of the image intensity distribution,

$$D_p(L_i) = -\ln P_I(I_p|L_i). \qquad (2)$$

The smoothness term $V_{p,q}$ is based on the intensity as well as on the image gradient C_x, constraining the shape of the cortex:

$$\begin{aligned} V_{p,q} &= c \cdot \left(\exp\left(-\frac{(I_p - I_q)^2}{2\sigma^2} \right) \cdot \frac{1}{\mathrm{dist}(p,q)} \right) \\ &+ (1-c) \cdot \left(1 - \max_{x \in N_{p,q}} (C_x) \right). \end{aligned} \qquad (3)$$

Parameter c controls the contribution of the boundary and intensity based parts. When $c = 1$, only the intensity discontinuity part has an influence and when $c = 0$, only the gradient term has an influence.

The first term in Eq. 3 penalizes intensity discontinuities and is based on the MRF. For every voxel in the brain volume, edges are positioned between the voxel and all its neighbouring voxels according to the chosen neighbourhood system. The weights are calculated by this first term, which consists of the squared intensity difference between the two voxels $(I_p - I_q)^2$, the intensity variance over the whole volume σ^2 and the distance dist(p, q) between both voxels. When the intensity difference is small, the weight will be large and vice versa. Consequently, the voxels with similar intensity values will less likely be separated from each other because the cost will be higher. Similarly, the voxels with largely differing intensities will be faster separated. The variance σ^2 is included to adapt between images with overall strongly differing intensity values and those with overall less differing intensity values. Finally, taking the spatial distance between neighboring voxels into account ensures that voxels that are further away contribute less to the neighbourhood system of the considered voxel.

The second term in Eq. 3 makes use of the image gradient C_x to constrain the shape of the cortex. The image gradient is computed for each voxel using the same neighbourhood system as is used in the first term. Afterwards, the mean gradient for the considered voxel is calculated. In the computation of the weight between two neighbouring voxels, the maximum mean gradient of the two voxels is used. By using the mean gradient, we reduce the noise influence.

III. Results

The performance of the proposed brain cortex segmentation method is validated quantitatively using brain phantom data and qualitatively using 8 real patients. In both cases only T1-W MRI volumes are used.

A. Quantitative validation

To validate the method quantitatively, we need images with known "ground truth". Thus, we used the simulated MR images from the realistic brain phantom, BrainWeb [14] ($181 \times 217 \times 181$ voxel matrix with a resolution of $1mm \times 1mm \times 1mm$). The results of our method (3DGC) were compared with the four methods: FSL, SPM, HBM and FCM. The Dice coefficient (ρ_{GM}) is used as a similarity measure.

$$\rho_{\mathrm{GM}} = \frac{2|A_i \bigcap B_i|}{|A_i| + |B_i|}, \tag{4}$$

where A_i and B_i denote the set of pixels labelled into i by the "ground truth" and segmentation method respectively, and $|A_i|$ denotes the number of elements in A_i. The dice coefficient was calculated as the mean value for the whole phantom volume. For the FSL and SPM the parameters were chosen to give the highest ρ_{GM}.

The segmentation results for four noise levels are shown in Fig. 3. The results show that our method 3DGC has higher ρ_{GM} values than the FSL, SPM, HMB and FCM for a range of different noise levels. Only for the lowest noise level, the HBM and FCM score higher.

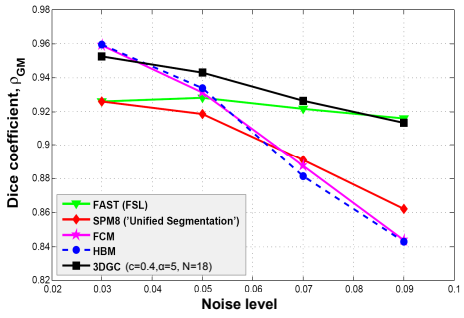

Fig. 3. The similarity measure ρ_{GM} of the brain cortex segmentation using the 3DGC, FSL, SPM, FCM and HBM methods for 4 different noise levels. In general, the 3DGC performs better than other methods, especially for higher noise levels.

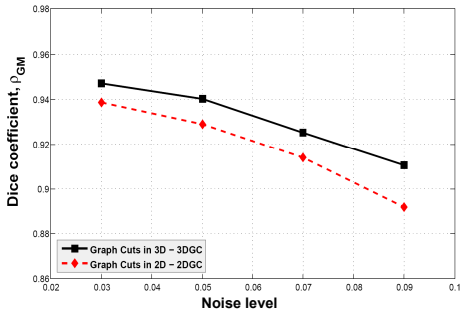

Fig. 4. The similarity measure ρ_{GM} of our method using 2D and 3D segmentation. We clearly see that the 3D segmentation gives better results for all considered noise levels.

In Fig. 4 we show that 3D graph cuts segmentation performs better than 2D (slice by slice) graph cuts segmentation. The similarity measure ρ_{GM} for every slice in the phantom volume is shown in Fig. 5. The graph shows a line for each of the noise levels.

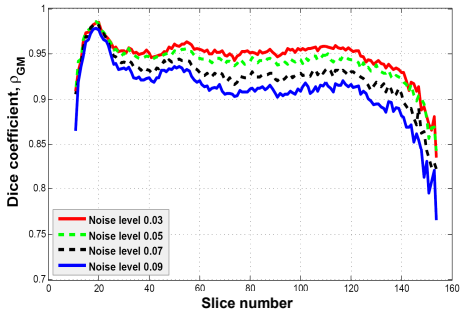

Fig. 5. The similarity measure ρ_{GM} of the 3DGC method for all slices of the phantom volume, for different noise levels. We see that ρ_{GM} is stable over a wide range of slice numbers, but drops in the higher regions of the brain.

Fig. 6 visualizes results of different segmentation methods of the phantom slice number 90 with the highest noise level (0.09). This is to illustrate the robustness of the different methods to noise. It is clear from Fig. 6 that the HBM and FCM have a lot of noise artifacts. The SPM shows less noise artifacts, while the FSL and 3DGC are most robust to noise.

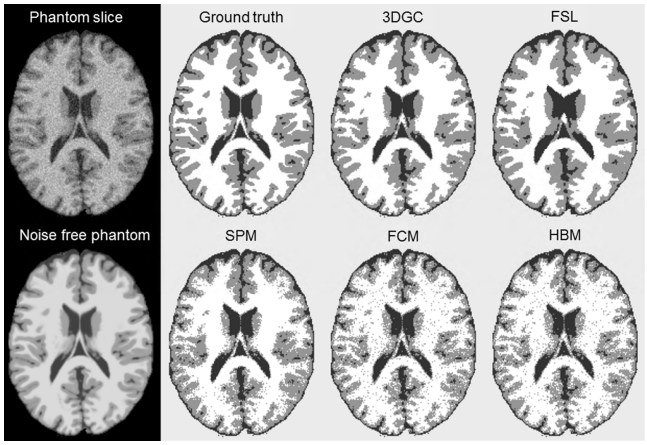

Fig. 6. The resulting segmentation of the phantom slice 90 with the highest noise level (0.09) is shown for the 4 different methods. The 3DGC and FSL show the closest resemblance to the ground truth, while the HBM, FCM and SPM retain more noise artifacts.

B. Qualitative validation

The qualitative validation was performed on 8 real patients with FCD lesions. The MRI were recorded at Ghent University Hospital on a Siemens 3T MRI scanner ($256 \times 256 \times 176$ voxel matrix with a resolution of $1mm \times 1mm \times 1mm$). The MRI were preprocessed by removing skull, lipid layers and bias field. The cortex segmentation is visually evaluated by expert physician. In all cases the segmentation was successful and the lesions were segmented as part of the cortex. The segmentation results are shown in Fig. 7 for four patients. The original MRI slice is shown at the left side with a rectangle around the lesion. At the right side, the segmented slice is shown in a similar way.

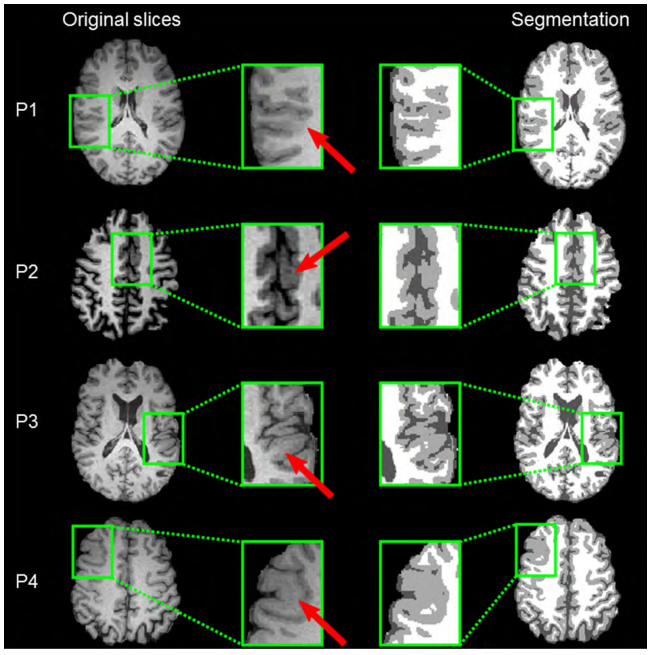

Fig. 7. The cortex segmentation results for four different patient are shown in each row. The original MRI slice is shown at the left and the resulting slice after segmentation with the 3DGC is shown at the right.

IV. Conclusion

We propose an improved technique for automatic 3D brain segmentation based on the graph cuts algorithm and MRF. Based on the quantitative validation, the proposed 3DGC method outperforms the popular brain segmentation techniques for a wide range of noise levels. Experimental results with different MRF neighbourhood systems showed that the 3D segmentation outperforms the 2D segmentation. The qualitative validation indicated the ability of the 3DGC to successfully segment the FCD lesions as a part of cortex, even when the λ parameter is not precisely tuned to the image. The results are very encouraging and demonstrate that the 3DGC can improve the FCD lesion detection and be successfully applied in many other practical applications. In future work, we will incorporate the multi-modal intensity information, from T1-W and Core Flair MRIs, to improve the performance of the 3DGC method.

References

[1] J. Rajan, K. Kannan, C. Kesavadas, B. Thomas, and A.K. Gupta, "Focal cortical dysplasia (fcd) lesion analysis with complex diffusion approach," *Comput Med Imaging Graph*, vol. 33, no. 7, 2009.

[2] A. Bernasconi, S.B. Antel, D.L. Collins, N. Bernasconi, A. Olivier, F. Dubeau, G.B. Pike, F. Andermann, and D.L. Arnold, "Texture analysis and morphological processing of magnetic resonance imaging assist detection of focal cortical dysplasia in extra-temporal partial epilepsy," *Annals of Neurology*, vol. 49, no. 6, pp. 770–775, 2001.

[3] S.B. Antel, A. Bernasconi, N. Bernasconi, D.L. Collins, R.E. Kearney, R. Shinghal, and D.L. Arnold, "Computational models of MRI characteristics of focal cortical dysplasia improve lesion detection," *NeuroImage*, vol. 17, pp. 1755–1760, 2002.

[4] O. Colliot, T. Mansi, N. Bernasconi, V. Naessens, D. Klironomos, and A. Bernasconi, "Segmentation of focal cortical dysplasia lesions using a feature-based level set," *MICCAI 2005*, vol. 3749, no. Pt 1, pp. 375–382, 2005.

[5] P. Besson, O. Colliot, A. Evans, and A. Bernasconi, "Automatic detection of subtle focal cortical dysplasia using surface-based features on MRI," *Proc. 5th IEEE ISBI Conference*, pp. 1633–1636, june 2008.

[6] Y. Zhang, M. Brady, and S. Smith, "Segmentation of brain MR images through a hidden markov random field model and the expectation-maximization algorithm," *IEEE Trans Med Imaging*, vol. 20, no. 1, pp. 45–57, 2001.

[7] J. Ashburner and K.J. Friston, "Unified segmentation," *NeuroImage*, vol. 26, no. 3, pp. 839–851, 2005.

[8] J.C. Bezdek, J.H. Gilmore, W. Lin, and G. Gerig, *Pattern Recognition with Fuzzy Objective Function Algorithms*, Plenum Press, New York, 1981.

[9] Y.Y. Boykov and M.P. Jolly, "Interactive graph cuts for optimal boundary and region segmentation of objects in N-D images," *Proc. 6th IEEE ICCV Conference*, pp. 105–112, 2001.

[10] Z. Song, N. Tustison, B. Avants, and J.C. GeeChan, "Integrated graph cuts for brain MRI segmentation," *MICCAI 2006*, vol. 4191, no. Pt 2, pp. 831–838, Sep. 2006.

[11] Y. Y. Boykov, O. Veksler, and R. Zabih, "Fast approximate energy minimization via graph cuts," *IEEE Transactions on PAMI*, vol. 23, no. 11, pp. 1222–1239, 2001.

[12] R. Wolz, R. A. Heckemann, P. Aljabar, A. Hajnal J.V. Hammers, J. Ltjnen, and D. Rueckert, "Measurement of hippocampal atrophy using 4D graph-cut segmentation: Application to ADNI," *NeuroImage*, vol. 52, pp. 109–118, 2010.

[13] A.A. D'Souza, "Using EM to estimate a probability density with a mixture of gaussians," 2004.

[14] D. L. Collins, A. P. Zijdenbos, V. Kollokian, J. G. Sled, N. J. Kabani, C. J. Holmes, and A. C. Evans, "Design and construction of a realistic digital brain phantom," *IEEE Trans. Med. Imag.*, vol. 17, pp. 463–468, 1998, http://www.bic.mni.mcgill.ca/brainweb/.